Heliyon 9 (2023) e13365

Contents lists available at ScienceDirect

Heliyon

journal homepage: www.cell.com/heliyon

Research article

Dual-wideband sandwich coupled three-lines bandpass filter based on modified open-stub loaded stepped impedance resonator with improved second harmonic for 5G wi-fi/ ku-band applications

Maroua Firmli *, Abdelkarim Zatni

Laboratory of Metrology and Information Processing (LMIP), Faculty of Science, Ibn Zohr University, B.P. 8106, 80000, Agadir, Morocco

ARTICLE INFO

Keywords:
OSL-TSIR
Three parallel coupled line
Dual-wideband bandpass filter
Microstrip
5G- wifi
Ku-band
Spurious resonant frequency
Selectivity

ABSTRACT

A modified open-stub-loaded three sections stepped impedance resonator (OSL-TSIR) is analysed in this paper. Based on the even- and odd-mode analysis technique, it can be easily achieved that the proposed OSL-TSIR have the advantage of improving spurious resonant mode frequencies. Besides, more degrees of freedom are provided to control the location of harmonics. A third order Chebyshev dual-wideband bandpass filter composed of cascade parallel sandwich coupled three-lines sections of types SC/CS and OSL-TSIR which act as multi-mode resonator was developed and the design procedure is described. To demonstrate the efficiency of the design process, DB-BPF operating at 5.15/12.58 GHz (2.45 f_0) and FBW of 19/5.7% for 5G Wi-Fi/Ku-band Applications is designed and simulated. Three transmission zeros are created, resulting in the excellent band-in-band isolation and high selectivity. The filter has a miniaturized size of 27 mm × 18 mm.

1. Introduction

Bandpass filter with multi-band or wide stopband response have attracted an important attention in modern wireless telecommunication system as a crucial building block that influence the demeanor of the entire system. For multi-band wireless communication system, dual-band bandpass filters are highly desirable during the last few decades and their resonators are the important key that can control characteristics performances of filter. Extensive structures of resonators such as stepped impedance resonator (SIR) [1–6], patch resonator [7,8], ring resonator [9,10], and stacked spiral resonator [12] have been constructed and developed in recent years to design dual bandpass filters. The main benefit of SIR is that the size of realised DB-BPF can be reduced. However, there are lacks of transmission zeros at upper and lower passbands which involve to a poor selectivity. Besides, narrow dual bandwidths are achieved. Using those simple configurations, it can be difficult to control centre frequencies and relative bandwidth. In order to avoid this problem, various structures of stub-loaded resonator are utilised to design filters [13–17].

Parallel coupled two-lines have been found to be very common for implementing bandpass filter with narrow bandwidth in many wireless telecommunication systems due to its major advantages include its cheap fabrication cost, simple design synthesis method and easier integration with other components. Nevertheless, the small gap of the coupling stage when a wide bandwidth filter is required (FBW>10%) presents the main limitation. To overcome this drawback, aperture backed parallel-coupled lines can be applied to enhance coupling gaps. However, this solution complicates the structure design analysis. The use of three parallel coupled lines section instead of the two ones can provide an effective solution to construct a wideband filter with improved coupling [18,19]. But, there are

* Corresponding author.
E-mail address: maroua.firmli@edu.uiz.ac.ma (M. Firmli).

https://doi.org/10.1016/j.heliyon.2023.e13365
Received 27 August 2022; Received in revised form 12 January 2023; Accepted 28 January 2023
Available online 9 February 2023
2405-8440/© 2023 The Authors. Published by Elsevier Ltd. This is an open access article under the CC BY-NC-ND license (http://creativecommons.org/licenses/by-nc-nd/4.0/).

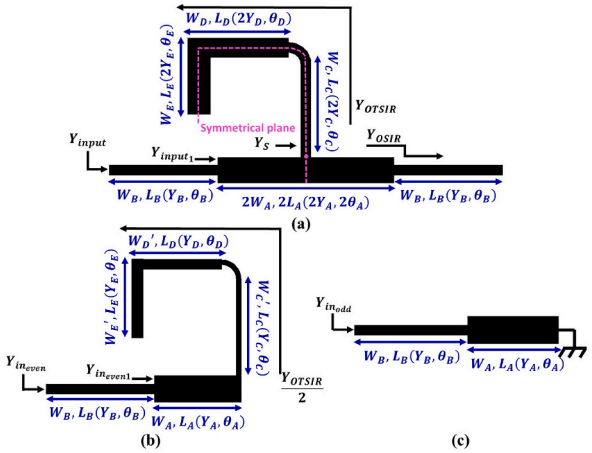

Fig. 1. a) Structure of the proposed OSL-TSIR. (b) Even -and (c) Odd-mode equivalent circuit.

still some deficiency for this type of structures, the most notably one of which is the poor selectivity, and also the poor harmonics suppression.

In this work a new dual-wideband parallel three coupled lines bandpass filter is studied and developed using OSL-TSIR. In compared with the SLR described in Refs. [13,15–17], the proposed resonator structure provides more degrees of freedom to flexibly in adjusting the locations of the resonant modes frequencies. Moreover, harmonic suppression characteristics of the analysed resonator are better than those in Ref. [14]. For validation, a detailed theoretical design procedure is presented and verified. Three transmission zeros are achieved, which leads to a very good band-in-band and high skirt selectivity.

1.1. Analysis of the proposed OSL-TSIR

Fig. 1 (a) depicts the structure model of the OSL-TSIR resonator considered in this paper. It is composed of three loaded open-circuited stepped impedance stubs connected to the open-ended quarter wavelength stepped impedance resonator at the midpoint. Y_m (m = A, B, C, D, E) and θ_m denote the characteristic admittance and electrical length of each transmission line section, respectively. The equivalent input admittance Y_{input} can be deduced, by applying the transmission line theory [20], as in the ensuing equation (1):

$$Y_{input} = Y_B \frac{Y_{input_1} + jY_B \tan\theta_B}{Y_B + jY_{input_1} \tan\theta_B} \tag{1}$$

Where, Y_{input_1}, Y_s, Y_{OTSIR}, Y_{OSIR} are defined by the equations (1.a), (1.b), (1.c) and (1.d):

$$Y_{input_1} = Y_A \frac{Y_S + jY_A \tan\theta_A}{Y_A + jY_S \tan\theta_A} \tag{1.a}$$

$$Y_S = Y_{OSIR} + Y_{OTSIR} \tag{1.b}$$

$$Y_{OTSIR} = 2Y_C \frac{2Y_C \tan\theta_C + j2Y_D \frac{2Y_D \tan\theta_D + 2Y_E \tan\theta_E}{2Y_D - 2Y_E \tan\theta_D \tan\theta_E}}{2Y_C - 2Y_D \frac{2Y_D \tan\theta_D + 2Y_E \tan\theta_E}{2Y_D - 2Y_E \tan\theta_D \tan\theta_E} \tan\theta_C} \tag{1.c}$$

$$Y_{OSIR} = jY_A \frac{Y_B \tan\theta_B + Y_A \tan\theta_A}{Y_A - Y_B \tan\theta_A \tan\theta_B} \tag{1.d}$$

To simplify the analysis, it is assumed that $Y_A = Y_C$, $\theta_D = \theta_E$, $R_{AB} = Y_A/Y_B$, $R_{DA} = Y_D/Y_A$ and $R_{EA} = Y_E/Y_A$.Thus, the final input admittance formula can be rewritten as in equation (2):

$$Y_{input} = jY_B \frac{\tan\theta_D(\alpha R_{EA} \tan\theta_D + \beta {R_{AB}}^2) + R_{DA} \tan\theta_B(\sigma \tan\theta_C + \mu \tan\theta_A) + R_{AB}R_{DA}(2\tan\theta_B + 3R_{AB} \tan\theta_A + 2R_{AB} \tan\theta_C)}{\tan\theta_D(\delta R_{EA} \tan\theta_D + \rho R_{AB}R_{DA}) + R_{DA} \tan\theta_B(\tau \tan\theta_C + \varepsilon \tan\theta_A) + R_{AB}R_{DA}(1-2\tan\theta_A \tan\theta_C - \tan{\theta_A}^2)} \tag{2}$$

where $\alpha, \beta, \sigma, \mu, \delta, \tau, \varepsilon$ *and* ρ are expressed by the equations (2.a), (2.b), (2.c), (2.d), (2.e), (2.f), (2.g) and (2.h):

$$\alpha = 2\tan\theta_A \tan\theta_B(\tan\theta_B + 2R_{AB} \tan\theta_C - \tan\theta_A \tan\theta_B \tan\theta_C + R_{AB} \tan\theta_A) - 2R_{AB} \tan\theta_B - 3{R_{AB}}^2 \tan\theta_A - 2{R_{AB}}^2 \tan\theta_C \tag{2.a}$$

$$\beta = 2{R_{DA}}^2 + 2R_{DA}R_{EA} - 2R_{DA} \tan\theta_A \tan\theta_C(R_{DA} + R_{EA}) \tag{2.b}$$

$$\sigma = 2\tan\theta_D((R_{DA} + R_{EA})(\tan\theta_A \tan\theta_B + R_{AB} \tan{\theta_A}^2 - R_{AB}) \tag{2.c}$$

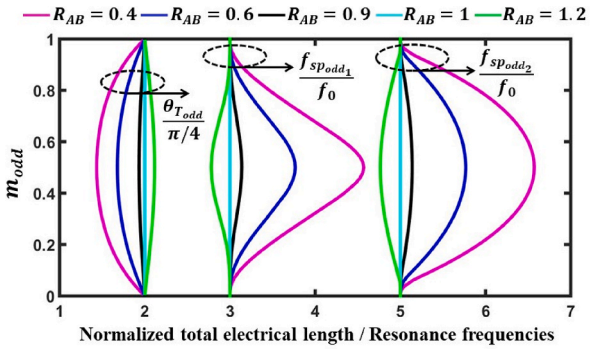

Fig. 2. Total electrical length and the normalized odd-mode spurious frequencies for several values of R_{AB}

$$\mu = 2\tan\theta_D((R_{DA}+R_{EA})(\tan\theta_A\tan\theta_B - 2R_{AB})) - 2(\tan\theta_B + R_{AB}\tan\theta_A) \tag{2.d}$$

$$\delta = \tan\theta_A\tan\theta_B(2 + 2{R_{AB}}^2 - R_{AB}\tan\theta_A\tan\theta_B - 2R_{AB}\tan\theta_B\tan\theta_C - 2\tan\theta_A\tan\theta_C) + R_{AB}(\tan{\theta_A}^2 + \tan{\theta_B}^2 + 2R_{AB}\tan\theta_B\tan\theta_C + 2\tan\theta_A\tan\theta_C) \tag{2.e}$$

$$\tau = \tan\theta_A\tan\theta_D((R_{DA}+R_{EA})(2 + 2{R_{AB}}^2 - R_{AB}\tan\theta_A\tan\theta_B)) + R_{AB}((R_{DA}+R_{EA})\tan\theta_B\tan\theta_D + 2(R_{DA}\tan{\theta_A}^2 + R_{AB}\tan\theta_A\tan\theta_B)) \tag{2.f}$$

$$\varepsilon = 2(R_{DA}+R_{EA})(\tan\theta_A\tan\theta_D + R_{AB}\tan\theta_B\tan\theta_D) - 2(1+{R_{AB}}^2) + R_{AB}R_{DA}(\tan\theta_A\tan\theta_B - 1) \tag{2.g}$$

$$\rho = (R_{DA}+R_{EA})(\tan{\theta_A}^2\tan\theta_c - \tan\theta_c - 2\tan\theta_A - 2R_{AB}\tan\theta_B) - R_{EA}\tan\theta_D \tag{2.h}$$

1.2. Even- and odd-mode resonant property

Due to the symmetrical topology of the suggested resonator about the plane of symmetry, the even- and odd-mode analysis technique can be employed to categorize it resonant characteristics frequencies. For the odd mode excitation, the three-section stepped impedance open-circuited stub can be considered as an electrical wall, the voltage is zero at the midpoint and the symmetrical plane turn into short circuited which leads to the equivalent stepped impedance resonator structure illustrated in Fig. 1 (c), where the imput admittance can be derived as in the equation (3) [21]:

$$Y_{inodd} = jY_B\frac{\tan\theta_A\tan\theta_B - R_{AB}}{\tan\theta_A + R_{AB}\tan\theta_B} \tag{3}$$

Therefore, resonant mode frequencies can be acquired by considering $Y_{inodd} = 0$:

$$\tan(m_{odd}\theta_{odd})\tan((1-m_{odd})\theta_{odd}) - \mathrm{R_{AB}} = 0 \tag{4}$$

Where m_{odd} is given in the equation (5),

$$m_{odd} = \theta_A/(\theta_A+\theta_B) = \theta_A/\theta_{Todd} \tag{5}$$

It can be distinguished from equation (4) that the odd-mode spurious resonant frequencies of the equivalent circuit can be controlled by tuning the values of the electrical length and the impedance ratios m_{odd} and R_{AB}, respectively. Since it is difficult to found an analytical solution to the given equation, a root-searching program based on the Newton's method is applied to calculate the resonant mode frequencies of the geometry. Fig. 2 plots curves of the total electrical length θ_{Todd} and the normalized odd-mode spurious frequencies $f_{sp\ odd\_1}/f_0$, $f_{sp\ odd\_2}/f_0$ with respect to f_0 versus different loaded point m_{odd} for several values of R_{AB}, where f_0, $f_{sp\ odd\_1}$ and $f_{sp\ odd\_2}$ are the fundamental resonant frequency, first and second spurious harmonics modes, respectively. As shown in Fig. 2, by increasing R_{AB}, θ_{Todd} increases. In another way, the normalized spurious harmonic mode shifts lower when R_{AB} increases, and higher when this last decreases.

For the even-mode excitation, the equivalent open-circuited model illustrated in Fig. 1 (b) is obtained by setting the symmetrical plane as a magnetic wall (there is no current flow via the symmetrical plane). Hence, the resulting characteristic input admittanc can be given as in equation (6) :

$$\begin{aligned} Y_{in_{even}} &= Y_B\frac{Y_{in_{even1}} + jY_B\tan\theta_B}{Y_B + jY_{in_{even1}}\tan\theta_B} \\ &= jY_B\frac{\tan\theta_D(R_{EA}\tan\theta_D\alpha_1 - R_{DA}\beta_1) + R_{DA}\sigma_1}{\tan\theta_D(R_{EA}\tan\theta_D\mu_1 - R_{DA}\delta_1) - R_{DA}\tau_1} \end{aligned} \tag{6}$$

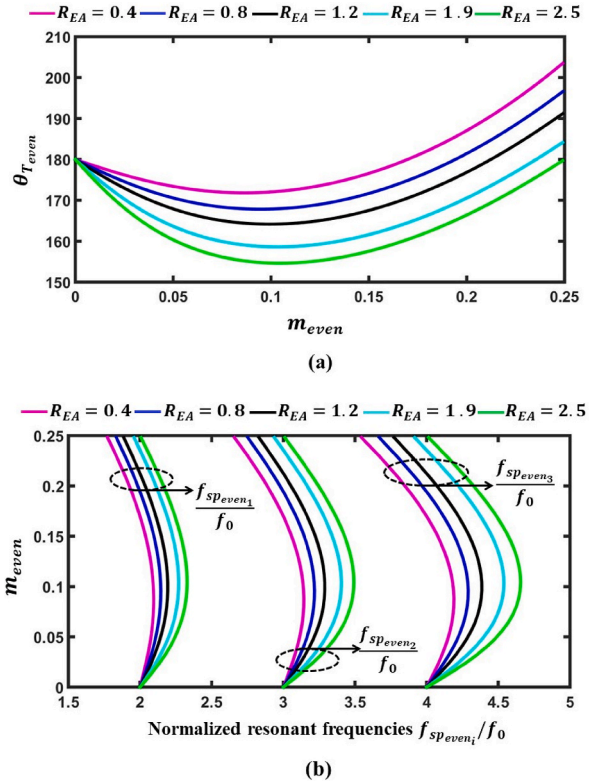

Fig. 3. (a) Total electrical length and (b) normalized spurious harmonics under length ratio for $R_{DA} = 2.5$ and $0 < R_{EA} < 2.5$

Where, the idmittance $Y_{in_{even_1}}$ and the coefficients α_1, β_1, σ_1, μ_1, δ_1, τ_1 are defined in the equations (6.a), (6.b), (6.c), (6.d), (6.e), (6.f) and (6.g),

$$Y_{in_{even_1}} = Y_A \frac{\frac{Y_{OTSIR}}{2} + jY_A \tan\theta_A}{Y_A + j\frac{Y_{OTSIR}}{2}\tan\theta_A} \tag{6.a}$$

$$\alpha_1 = \tan\theta_C(\tan\theta_A \tan\theta_B - 1) - \tan\theta_A \tan\theta_B \tag{6.b}$$

$$\beta_1 = \tan\theta_C((\tan\theta_A + \tan\theta_B)(R_{DA} + R_{EA})) + (\tan\theta_A \tan\theta_B - 1)(R_{DA} + R_{EA}) \tag{6.c}$$

$$\sigma_1 = R_{DA}(\tan\theta_B(1 - \tan\theta_A \tan\theta_C) + \tan\theta_A + \tan\theta_C) \tag{6.d}$$

$$\mu_1 = \tan\theta_C(\tan\theta_A + \tan\theta_B) + \tan\theta_A \tan\theta_B - 1 \tag{6.e}$$

$$\delta_1 = \tan\theta_C((\tan\theta_A \tan\theta_B + 1)(R_{DA} + R_{EA})) + (\tan\theta_A + \tan\theta_B)(R_{DA} + R_{EA}) \tag{6.f}$$

$$\tau_1 = R_{DA}(\tan\theta_B(\tan\theta_C - \tan\theta_A) + \tan\theta_A \tan\theta_C - 1) \tag{6.g}$$

Likewise, the resonant even-modes condition could be determined by considering $Y_{ineven} = 0$:

$$(R_{DA} - R_{EA}\tan\theta_D{}^2)\tan(\theta_A + \theta_B + \theta_C) + (R_{DA}R_{EA} + R_{DA}{}^2)\tan\theta_D = 0 \tag{7}$$

Where, $Y_A = Y_B$ is assumed for simplicity ensurement. In view of the fact that there are four electrical lengths θ_A, θ_B, θ_C and θ_D, the resulting formula can be solved by defining an even length ratio $m_{even} = \theta_D/(\theta_A + \theta_B + \theta_C + 2\theta_D) = \theta_D/\theta_{Teven}$, where θ_{Teven} is the total electrical length for the even-mode equivalent circuit. Accordingly, the equation (7) can be deduced as (8):

$$(R_{DA} - R_{EA}\tan(\theta_{T_{even}} m_{even})^2)\tan(\theta_{T_{even}}(1 - m_{even})) + (R_{DA}R_{EA} + R_{DA}{}^2)\tan(\theta_{T_{even}} m_{even}) = 0 \tag{8}$$

Solutions to (8) accorded to the even-mode resonance frequencies are dependent on the choice of three arbitrary parameters; R_{DA}, R_{EA}, and m_{odd}. Fig. 3, Figs. 4 and 5 depict the calculated total length θ_{Teven} and the normalized even-mode spurious resonant frequencies $f_{sp\ even\_1}/f_0$, $f_{sp\ even\_2}/f_0$, $f_{sp\ even\_3}/f_0$ with respect to f_0 under m_{even} for different values of impedance ratios R_{DA} and R_{EA}, respectively.As it can be observed, three cases are distinguished. For the first case, R_{DA} is fixed at 2.5, while the value of R_{EA} is adjusted to be varied

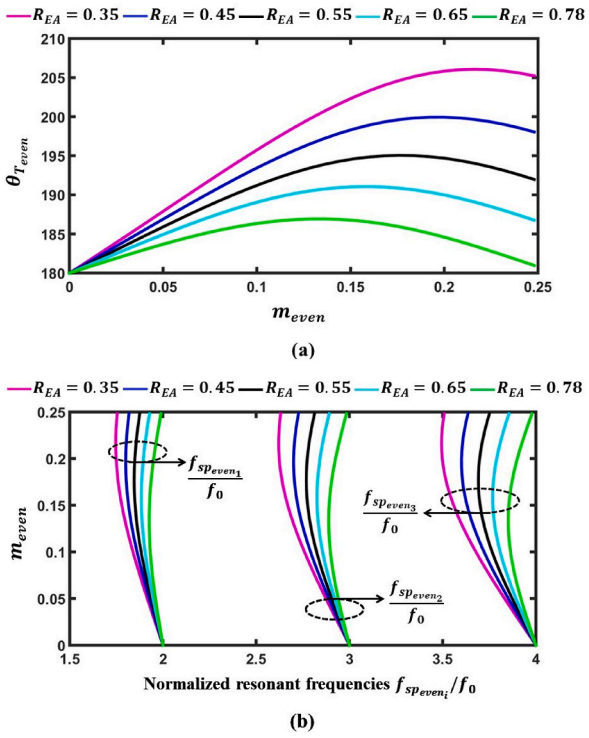

Fig. 4. (a) Total electrical length and (b) normalized spurious harmonics under length ratio for $R_{DA} = 0.8$ and $0 < R_{EA} < 1$

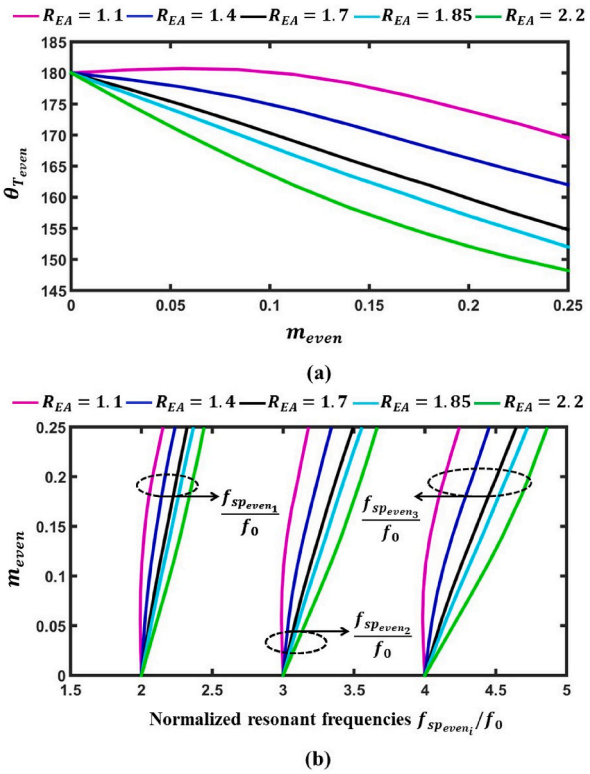

Fig. 5. (a) Total electrical length and (b) normalized spurious harmonics under length ratio for $R_{DA} = 0.8$ and $1 < R_{EA} < 2.5$

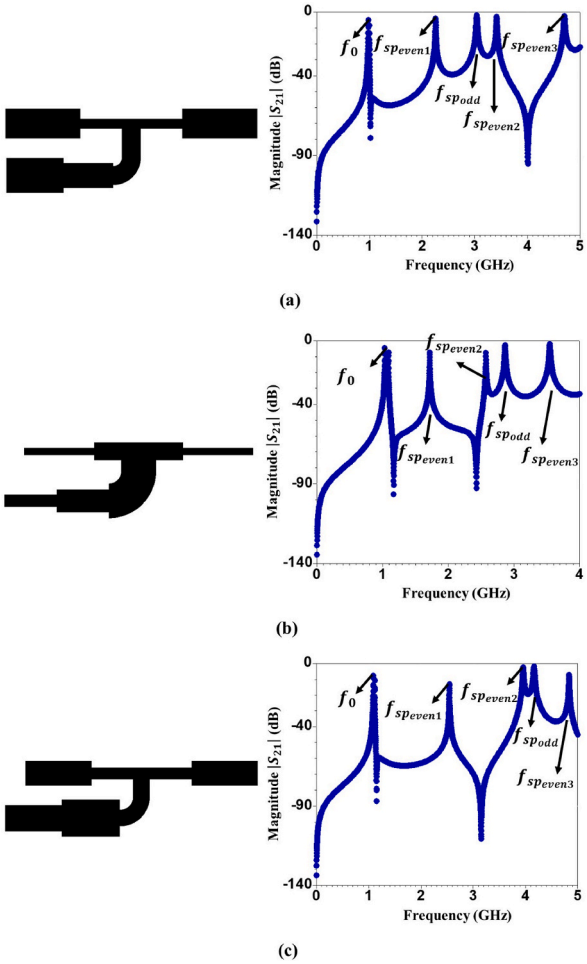

Fig. 6. Geometric configuration and simulated response frequency for (a) case A (b) case B and (c) case C.

Table 1
Comparaison of calculated spurious resonant frequencies against simulated ones.

Parameters specifications		$f_{sp\ even\_1}$		$f_{sp\ odd}$		$f_{sp\ even\_2}$		$f_{sp\ even\_3}$	
		Calculated	Simulated	Calculated	Simulated	Calculated	Simulated	Calculated	Simulated
A	$m_{odd} = 0.2$; $R_{AB} = 0.8$ $m_{even} = 0.135$ $R_{DC} = 1.2$; $R_{EC} = 2.5$	2.279	2.255	3.114	3.113	3.419	3.408	4.561	4.66
B	$m_{odd} = 0.2$; $R_{AB} = 2$ $m_{even} = 0.232$ $R_{EC} = 0.3$; $R_{DC} = 0.8$	1.717	1.718	2.9035	2.9	2.575	2.57	3.86	3.588
C	$m_{odd} = 0.3$; $R_{AB} = 0.3$ $m_{even} = 0.1$ $R_{DC} = 5$; $R_{EC} = 4$	2.553	2.553	4.32	4.32	3.83	4.06	5.107	4.866

between 0 and 2.5. As plotted in Fig. 3 (a), θ_{Teven} decreases as R_{EA} increases. Proportionally, as showen in Fig. 3 (b), the normalized spurious harmonics become larger when increasing R_{EA}. By choosing $R_{DA} = 0.8$ and R_{EA} that is ranging between 0 and 1, it can be shown from Fig. 4 (a,b) that the smaller R_{EA} is, the longer θ_{Teven} is, and the normalized spurious harmonic mode shift higher when R_{EA} increases, respectively. As illustrated in Fig. 5 (a) and Fig. 5 (b), by considering that $R_{DA} = 0.8$ and $1 < R_{EA} < 2.5$, the total longitudinal electrical length and normalized frequencies ratios become shorter and higher, respectively, when R_{EA} increases. Overall, to achieve a great length reduction and a hight spurious harmonic, it is required to choose R_{AB} as small as possible ($R_{AB} < 1$) and R_{EA} as large as possible. Let's notice that to obtain a realizable resonator, R_{AB} and R_{EA} cannot be selected so smaller or so larger since it creates a very large discontinuity and radiation losses.

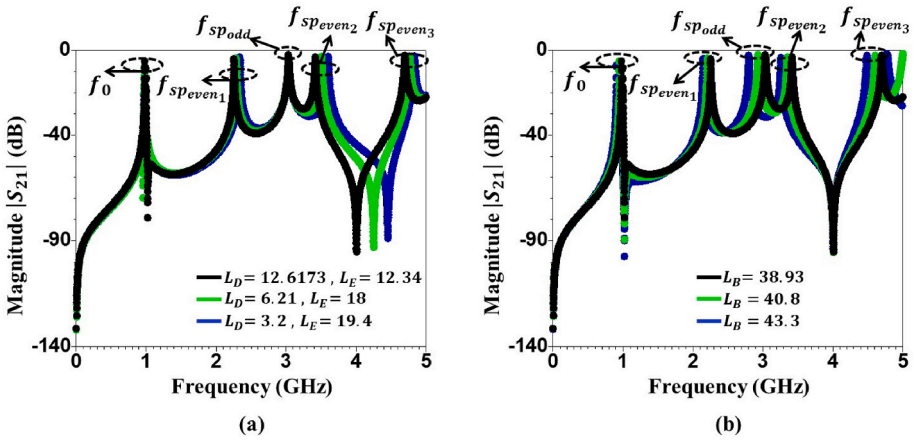

Fig. 7. Effect of L_B, L_D and L_E on the splitting of even-odd mode resonant frequencies.

1.3. Validation of theory

As a means to demonstrate the validity of the theoretical study derived in the previous sections, several structures of OSL-TSIR and the frequency distributions for different cases are simulated under the selected gap of 0.5 mm at the two sides in order to avoid the modification of their resonant frequencies as shown in Fig. 6 (a), Fig. 6 (b) and Fig. 6 (c), respectively. Table 1 lists the Comparaison of the predicted spurious resonant frequencies against simulated ones, and a good agreement can be observed.

Fig. 7 depicts the simulated frequency response of the proposed resonator for the first case under different length of $L_B(\theta_B)$, $L_D(\theta_D)$ and $L_E(\theta_E)$. It can be clearly verified from Fig. 7 (a), that by increasing L_E and decreasing L_D simultaneously, even-mode frequencies at $f_{sp\ even\_1}$, $f_{sp\ even\_2}$ and $f_{sp\ even\_3}$ are shifted, whereas the odd-mode $f_{sp\ odd\_1}$ keep unchanged. On the other hand, when L_B is changed, both even and odd-mode frequencies are affected as shown in Fig. 7 (b). Hence, those results demonstrate the even-odd mode analysis study discussed above.

1.4. Admittance slope parameter of the OSL-TSIR resonator

To establish the resonance features of any resonator it is appropriable to specify its slop parameter and its resonant frequency [21]. For the OSL-TSIR considered in this paper, the admittance slope parameter can be expressed as in the following equation (9):

$$b_r = \frac{Y_B}{2}\frac{X.Y + x.y}{(y)^2} \tag{9}$$

Where, the coefficients X, Y, x, y, A, B, C, D, A', B', C', D' and E' are derived as in (9.a)-(9.n):

$$X = R_{EA}\tan\theta_D\left(\frac{2\delta\theta_D}{\cos\theta_D{}^2} + A\tan\theta_D\right) + \tau R_{DA}(\theta_B\sec\theta_B{}^2\tan\theta_C + \theta_C\sec\theta_C{}^2\tan\theta_B) + BR_{DA}\tan\theta_B\tan\theta_C + \varepsilon R_{DA}(\theta_B\sec\theta_B{}^2\tan\theta_A + \theta_A\sec\theta_A{}^2\tan\theta_B) + CR_{DA}\tan\theta_B\tan\theta_A + R_{DA}R_{AB}(\rho\theta_D\sec\theta_D{}^2 + D\tan\theta_D) - ER_{AB}R_{DA} \tag{9.a}$$

$$Y = \tan\theta_D(\alpha R_{EA}\tan\theta_D + \beta R_{AB}{}^2) + R_{DA}\tan\theta_B(\sigma\tan\theta_C + \mu\tan\theta_A) + R_{AB}R_{DA}(2\tan\theta_B + 3R_{AB}\tan\theta_A + 2R_{AB}\tan\theta_C) \tag{9.b}$$

$$x = R_{EA}\tan\theta_D\left(\frac{2R_{EA}\alpha\theta_D}{\cos\theta_D{}^2} + A'\tan\theta_D\right) + \sigma R_{DA}(\theta_B\sec\theta_B{}^2\tan\theta_C + \theta_C\sec\theta_C{}^2\tan\theta_B) + B'R_{DA}\tan\theta_B\tan\theta_C + \mu R_{DA}(\theta_B\tan\theta_A \sec\theta_B{}^2 + \theta_A\sec\theta_A{}^2\tan\theta_B) + C'R_{DA}\tan\theta_B\tan\theta_A + \beta R_{AB}{}^2\theta_D\sec\theta_D{}^2 + D'R_{AB}{}^2\tan\theta_D + E'R_{AB}R_{DA} \tag{9.c}$$

$$y = \tan\theta_D(\delta R_{EA}\tan\theta_D + \rho R_{AB}R_{DA}) + R_{DA}\tan\theta_B(\tau\tan\theta_C + \varepsilon\tan\theta_A) + R_{AB}R_{DA}(1 - 2\tan\theta_A\tan\theta_C - \tan\theta_A{}^2) \tag{9.d}$$

$$A = 2\theta_A\sec\theta_A{}^2(R_{AB}\tan\theta_A + R_{AB}\tan\theta_C + \tan\theta_B - 2\tan\theta_A\tan\theta_B\tan\theta_C + R_{AB}{}^2\tan\theta_B - R_{AB}\tan\theta_A\tan\theta_B{}^2 - R_{AB}\tan\theta_B{}^2\tan\theta_C) + 2\theta_C\sec\theta_C{}^2(R_{AB}\tan\theta_A + R_{AB}{}^2\tan\theta_B - \tan\theta_A{}^2\tan\theta_B) + 2\theta_B\sec\theta_B{}^2(R_{AB}\tan\theta_B + R_{AB}{}^2\tan\theta_C + \tan\theta_A - \tan\theta_C\tan\theta_A{}^2 + R_{AB}{}^2\tan\theta_A - R_{AB}\tan\theta_A{}^2\tan\theta_B - 2R_{AB}\tan\theta_A\tan\theta_B\tan\theta_C - 2R_{AB}\tan\theta_A\tan\theta_B{}^2) \tag{9.e}$$

$$B = ((\theta_A\sec\theta_A{}^2\tan\theta_D + \theta_D\sec\theta_D{}^2\tan\theta_A)((R_{DA} + R_{EA})(2(R_{DA}{}^2 + 1) - \mathrm{R_{AB}}\tan\theta_A\tan\theta_B)) - \tan\theta_A\tan\theta_D(R_{AB}(R_{DA} + R_{EA})(\theta_A \tan\theta_B\sec\theta_A{}^2 + \theta_B\sec\theta_B{}^2\tan\theta_A)) + 2R_{AB}(2R_{DA}\theta_A\sec\theta_A{}^2\tan\theta_A + \theta_A\sec\theta_A{}^2\tan\theta_B + \theta_B\sec\theta_B{}^2\tan\theta_A) + R_{AB}(R_{DA} + R_{EA}) (\theta_D\sec\theta_D{}^2\tan\theta_B + \theta_B\sec\theta_B{}^2\tan\theta_D) \tag{9.f}$$

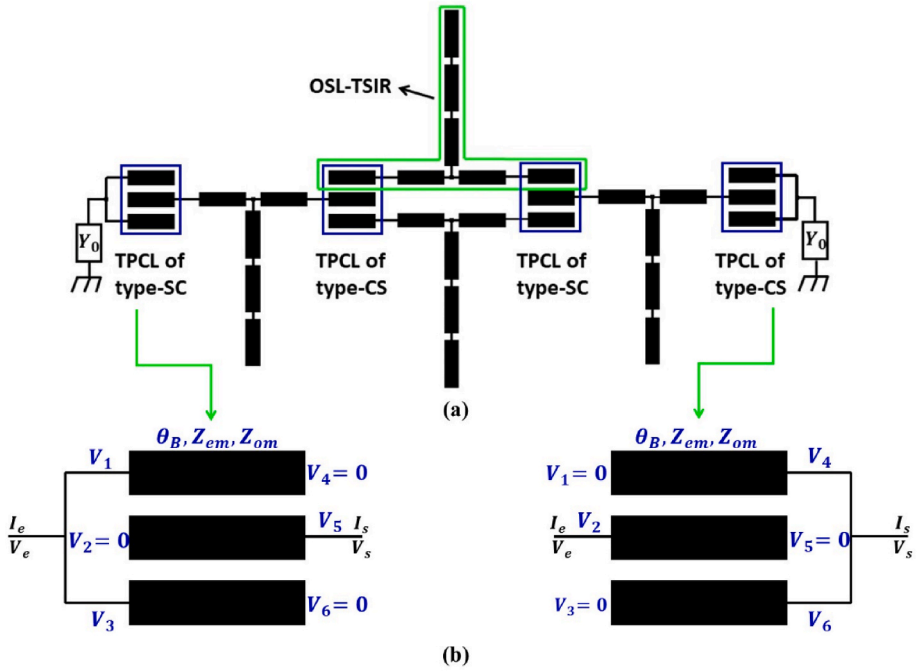

Fig. 8. (a) Ideal electrical circuit of the proposed filter. (b) Schematic of the applied sandwich coupled lines of type SC and CS.

$$C = 2(\theta_A \sec \theta_A{}^2 \tan \theta_D + \theta_D \sec \theta_D{}^2 \tan \theta_A + R_{AB}\theta_B \sec \theta_B{}^2 \tan \theta_D + R_{AB}\theta_D \sec \theta_D{}^2 \tan \theta_B)(R_{DA} + R_{EA}) + R_{DA}R_{AB}(\theta_B \tan \theta_A \sec \theta_B{}^2 + \theta_A \sec \theta_A{}^2 \tan \theta_B) \quad (9.g)$$

$$D = (R_{DA} + R_{EA})(\theta_C \sec \theta_C{}^2 \tan \theta_A{}^2 + 2\theta_A \sec \theta_A{}^2 \tan \theta_A \tan \theta_c - \theta_C \sec \theta_C{}^2 - 2\theta_A \sec \theta_A{}^2 - 2R_{AB}\theta_B \sec \theta_B{}^2) - R_{EA}\theta_D \sec \theta_D{}^2 \quad (9.h)$$

$$E = 2(\theta_C \sec \theta_C{}^2 \tan \theta_A + \theta_A \sec \theta_A{}^2 \tan \theta_C - \theta_A \sec \theta_A{}^2 \tan \theta_A) \quad (9.i)$$

$$A' = \theta_A \sec \theta_A{}^2(2 \tan \theta_B{}^2 + 4R_{AB} \tan \theta_C \tan \theta_B - 4 \tan \theta_A \tan \theta_B{}^2 \tan \theta_C + 4R_{AB} \tan \theta_A \tan \theta_B - 3R_{AB}{}^2) + 2 \tan \theta_A \tan \theta_B(2\theta_B \sec \theta_B{}^2 + 2R_{AB}\theta_C \sec \theta_C{}^2 - \theta_C \sec \theta_C{}^2 \tan \theta_A \tan \theta_B - 2\theta_B \sec \theta_B{}^2 \tan \theta_A \tan \theta_C) + 2\theta_B \sec \theta_B{}^2(2R_{AB} \tan \theta_A \tan \theta_C - R_{AB} + R_{AB} \tan \theta_A{}^2) - 2R_{AB}{}^2\theta_C \sec \theta_C{}^2 \quad (9.j)$$

$$B' = \theta_D \sec \theta_D{}^2(2(R_{DA} + R_{EA})(\tan \theta_A \tan \theta_B - \mathrm{R_{AB}} + \mathrm{R_{AB}} \tan \theta_A{}^2)) + \theta_A \sec \theta_A{}^2(2(R_{DA} + R_{EA}) \tan \theta_D \tan \theta_B + 4\mathrm{R_{AB}} \tan \theta_D \tan \theta_A (R_{DA} + R_{EA}) + 4\mathrm{R_{AB}}(R_{DA} \tan \theta_B \tan \theta_A - 1)) + \theta_B \sec \theta_B{}^2(2(R_{DA} + R_{EA}) \tan \theta_D \tan \theta_A + 2\mathrm{R_{AB}}R_{DA} \tan \theta_A{}^2) \quad (9.k)$$

$$C' = 2\theta_D \sec \theta_D{}^2((R_{DA} + R_{EA})(\tan \theta_B \tan \theta_A - 2R_{AB})) + 2 \tan \theta_D(R_{DA} + R_{EA})(\theta_A \sec \theta_A{}^2 \tan \theta_B - \theta_B \sec \theta_B{}^2 \tan \theta_A) - 2(\theta_B \sec \theta_B{}^2 + R_{AB}\theta_A \sec \theta_A{}^2)) \quad (9.l)$$

$$D' = -2R_{DA}(\theta_A \sec \theta_A{}^2 \tan \theta_c + \theta_C \sec \theta_C{}^2 \tan \theta_A)(R_{DA} + R_{EA}) \quad (9.m)$$

$$E' = 2\theta_B \sec \theta_B{}^2 + 2R_{AB}\theta_C \sec \theta_C{}^2 + 3R_{AB}\theta_A \sec \theta_A{}^2 \quad (9.n)$$

2. Design procedure of the proposed dual-band TPC-OSL-TSIR bandpass filter

2.1. Equivalent circuit and design theory

Fig. 8 (a) displays the ideal electrical circuit of the proposed third -order dual bandpass filter which is basically composed of cascade parallel coupled three-lines sections and the OSL-TSIR resonator analysed in above sections.

As shown in Fig. 8 (b), and by imposing some conditions at terminal voltages and currents $V_{i=1,2,\ldots,6}$ and $I_{j=1,2,\ldots,6}$, respectively, there are two possible types of parallel three coupled-lines; type-SC where ports 1 and 3 are connected to each other as input port (V_e, I_e) whereas port 4 is set as output port (V_s, I_s) and type-CS where port 2 is considered to be the input port, while ports 4 and 6 are allocated as output port. Accordingly, the ABCD matrices of the equivalent two-port network can be derived from Refs. [22,23] as in the equations (10) and (11):

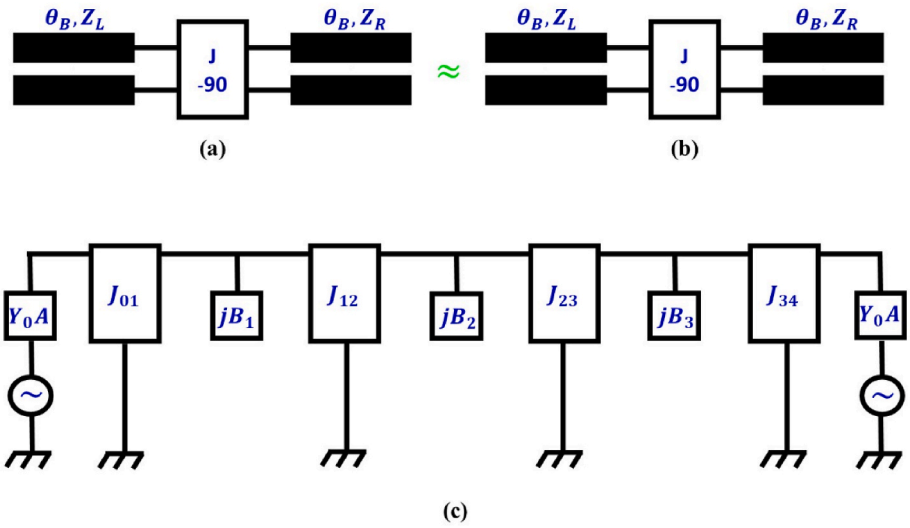

Fig. 9. Equivalent J-inverter circuit of Three coupled lines section. (b) Approximated J-inverter. (c) Equivalent circuit of the whole proposed dual-band BPF.

$$[ABCD]_{SC} = \begin{bmatrix} a\cos(\theta_B) & jb \\ jc\sin(\theta_B) & d\cos(\theta_B) \end{bmatrix} \tag{10}$$

$$[ABCD]_{CS} = \begin{bmatrix} d\cos(\theta_B) & jb \\ jc\sin(\theta_B) & a\cos(\theta_B) \end{bmatrix} \tag{11}$$

where,

$$a = \frac{Z_{em} + Z_{om}}{\eta_1 Z_{em} - \eta_2 Z_{om}}$$

$$b = \frac{(\eta_1 Z_{em} - \eta_2 Z_{om})^2 - (\eta_1{}^2 Z_{em}{}^2 + \eta_2{}^2 Z_{om}{}^2 + \eta_1 Z_{em} Z_{om} + \eta_2 Z_{em} Z_{om})\cos\theta_B}{(\eta_1 Z_{em} - \eta_2 Z_{om})\sin\theta_B}$$

$$c = \frac{1}{\eta_1 Z_{em} - \eta_2 Z_{om}}$$

$$d = \frac{\eta_1{}^2 Z_{em} + \eta_2{}^2 Z_{om}}{\eta_1 Z_{em} - \eta_2 Z_{om}}$$

$$\eta_1\eta_2 = -2, Z_{em} = \frac{Z_{ee}}{2 + \eta_1{}^2}, Z_{om} = \frac{Z_{oo}}{2 + \eta_2{}^2}$$

By following the approximation applied in Ref. [18] to create the equivalence between the coupled stages in Fig. 8 (b) and the equivalent J-inverter circuits shown in Fig. 9 (a,b), the generalized even- and odd-mode characteristic impedances expressions for each coupled-line section with arbitrary length can be determined as in (12) and (13):

$$\eta_1 Z_{em} = \frac{Z_0}{2}\frac{(JZ_0)^2 + (JZ_0)\csc\theta_B + 1}{1 - (JZ_0)^2\cot\theta_B} \tag{12}$$

$$\eta_2 Z_{om} = \frac{Z_0}{2}\frac{(JZ_0)^2 - (JZ_0)\csc\theta_B + 1}{1 - (JZ_0)^2\cot\theta_B} \tag{13}$$

Once the equivalence between the coupled stage and the J-inverter circuit is obtained, the third-order three-line bandpass filter in Fig. 8 (a) can be further approximated by the equivalent circuit shown in Fig. 9 (c). Thus, the admittance inverter parameter values $j_{j,j+1}$ can be derived by the formulas expressed in Refs. [24,25].

3. Results and discussion

With the help of the derived formulas and to demonstrate their validity, a third order Chebyshev dual-band parallel three coupled

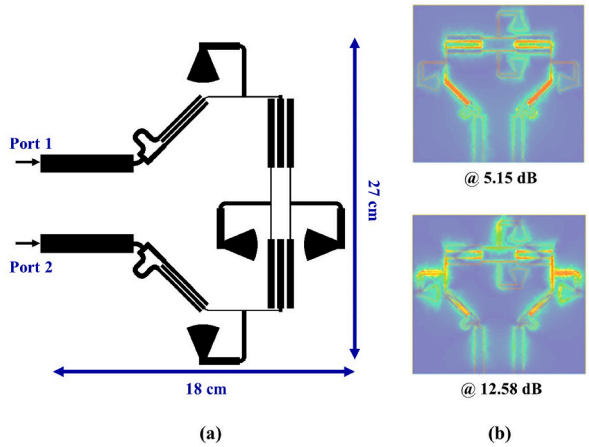

Fig. 10. (a) Layout of the proposed third-order parallel three coupled lines dual BPF using OSL-TSIR and (b) its E-field distribution at the two passband frequencies.

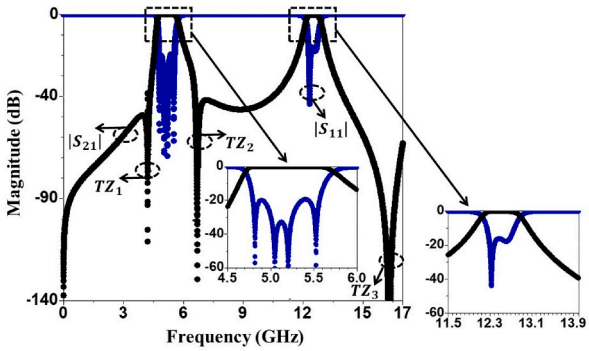

Fig. 11. Simulated results of the designed dual-wideband bandpass filter.

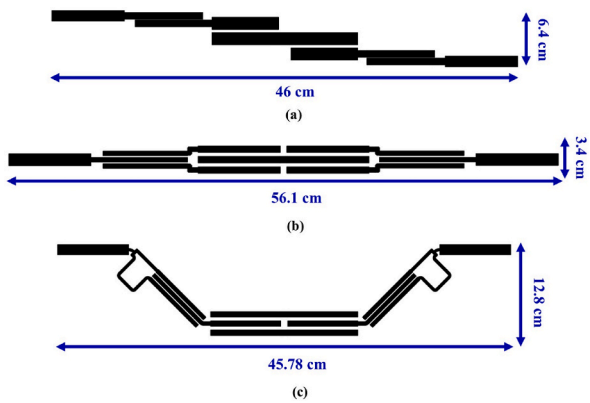

Fig. 12. (a) Conventional parallel coupled bandpass filter. (b) Conventional parallel coupled three lines bandpass filter-type 1. (c) Modified parallel coupled three lines bandpass filter-type type 2.

line OSL-TSIR bandpass filter with 0.5 dB passband ripple level was designed. The filter was implemented on Roger's RT/Duriod 5880 substrate having a relative permittivity of 2.2, a dielectric loss tangent of 9.10^{-4} , a copper thickness of 17.10^{-3} mm and substrate thickness of 0.508 mm in microstrip technology.The layout of the designed filter with an overall size of 27 mm $\times$ 18 mm is shown in Fig. 10 (a). Fig. 10 (b) depicts the electric-field distribution on the surface at the two center frequencies, the stronger coupling effect is presented by red color, whereas the feeble one is indicated by blue color. As it can be seen, the maximum of the current at the first passband is observed around the open-ended stepped impedance resonator, while the surface current at the second passband is strong

Table 2
Advantages of the proposed parallel coupled BPF compared with conventional ones.

Filter type	Input/output Gap size (mm)	IL (dB) at f_0	RL (dB) at f_0	Spurious frequency	TZs	size (mm^2)
Conventional parallel coupled BPF	0.0534	0.105	27.7	$\approx 2f_0$	0	46 × 6.4
Conventional parallel coupled three lines BPF of type1	0.203	0.209	13.492	$\approx 2f_0$	0	56.1 × 3.4
Modified parallel coupled three lines BPF of type 2	0.203	0.1	17.4	$\approx 2f_0$	2	45.78 × 12.8
Proposed filter with OSL-TSIR	0.12	0.022	34.005	$\approx 2.45f_0$	3	27 × 18

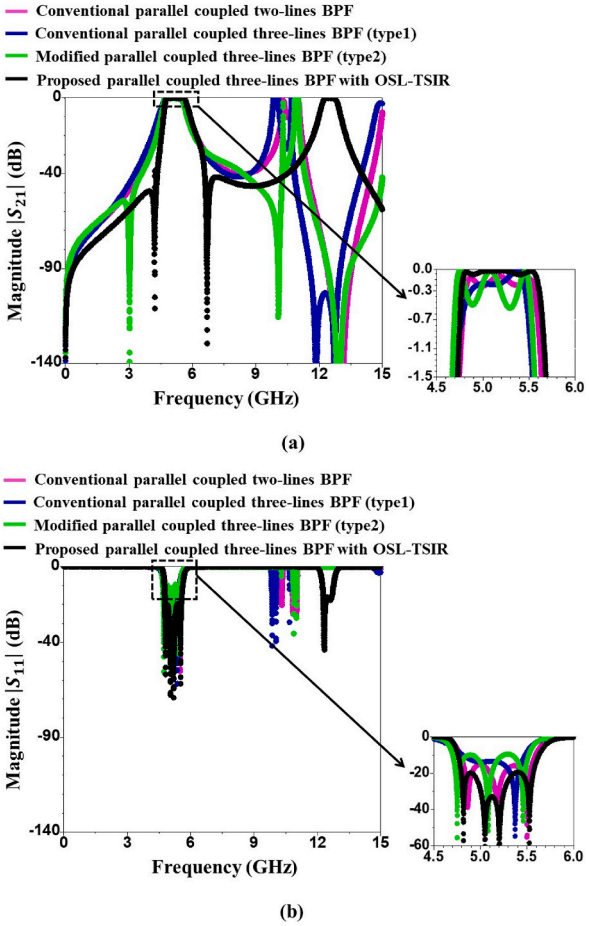

Fig. 13. Comparaison of (a) simulated S_{21} and (b) simulated S_{11} filtering performance of proposed filter with other parallel coupled line.

at the whole OSL-TSIR, which justify the use of the proposed multimode resonator and his effect on the construction of a multi-band response.

The simulated filtering performances are exhibited in Fig. 11. As can be observed, the center frequency of the spurious passband is located at 2.45 f_0 and then two passbands are achieved at 5.15/12.58 GHz with a fractional bandwidth of 19% and 5.7%, respectively. The minimum in-band insertion loss in the two passbands is found to be lower than 0.071 dB and 0.276 dB, while the return loss is better than 19.335 dB and 16.21 dB. Three transmission zeros at 4.246, 6.673 and 16.34 GHz are created, which improve the selectivity of the proposed BPF. The rejection level in the lower/upper stopband is better than 49.197 dB/41.814 dB, respectively, which led to get a verry good band-to-band isolations between the two passbands.

A comparative study between the proposed parallel bandpass filter and the existing ones in Fig. 12(a–c) is shown in Table 2. It obvious from the simulated results in Fig. 13 (a,b) that by the use of parallel three coupled lines instead of the two coupled sections provide an effective method to enlarging the gap size (from 0.0534 mm to 0.12 mm), and then the problem of limited fractional bandwidth (<10%) and hight fabrication cost can be solved.

On the other hand, the proposed BPF present a high skirt selectivity, low insertion loss and hight return loss in compared with the

Table 3
Comparaison of the proposed parallel coupled BPF with other reported dual-band BPF.

Reference	CFs	FBW (%)	Second passband CF	***IL*** **(*dB*)**	RL (dB)	Band-in-band isolation between the two passbands	TZs	Size (mm^2)
[11]	2.4/5.2	6.3/ 3.43	$\approx 2.17f_0$	–	>15/> 15	Good (> 30 dB)	1	24 × 30
[26]	7.89/ 8.892	3.43/4	$\approx 1.13f_0$	1.5/1.9	15/12	Poor (> 19 dB)	4	30.5 × 30
[27]	3.5/5.25	6.5/4.3	$\approx 1.5f_0$	1.87/2.33	>20/> 20	Good (> 40 dB)	2	27 × 19
[28] BPF_2	2.44/ 3.55	5.35/ 5.85	$\approx 1.46f_0$	2.17/1.71	10.32/10.32	Poor (> 15 dB)	3	53.7 × 23.15
[29]	1.8/2.4	–	$\approx 1.34f_0$	1/1.1	22/20	Good (> 40 dB)	3	35 × 45
[30]	2.4/5.2	10.5/ 5.5	$\approx 2.17f_0$	1.37/1.23	32/19	Poor (> 15 dB)	–	–
Proposed filter	5.15/ 12.58	19/5.7	$\approx 2.45f_0$	<0.071/< 0.276	>19.335/> 16.21	Very good (> 42 dB)	3	27 × 18

conventional three-edge coupled lines filter of type1 and miniaturized size of 17.06% as compared with the modified parallel coupled three lines BPF of type 2. Furthermore, the introduced OSL-TSIR resonator can be controlled to improve the spurious center frequency, which is pushed from 2 f_0 to 2.45 f_0.

Table 3 shows the performance comparison of recently reported dual-band BPFs and the proposed one. Distinctly, the proposed dual-band BPF has the advantages of high return loss, low insertion loss, excellent band-in-band isolation, high selectivity, wider relative bandwidth and compact size.

4. Conclusion

This work has presented a complete study of a novel dual-wideband bandpass filter based on parallel three coupled lines and a modified multi-mode resonator, which is consist of stepped impedance resonator with three loaded open stubs in the middle. The resonator has been analytically analysed by employing even-odd-mode technique, and spurious harmonics can be controlled by adjusting electrical length and impedance ratios. For a proof-of -concept, a third order Chebyshev dual-band parallel three coupled line OSL-TSIR bandpass filter for 5G-wifi/Ku-band applications was designed. The reported performance provides a low insertion loss, hight return loss, hight band-to-band isolation and selectivity and compact size.

Declarations

Author contribution statement

Maroua Firmli: Conceived and designed the experiments; Performed the experiments; Analysed and interpreted the data; Contributed reagents, materials, analysis tools or data; Wrote the paper.Abdelkarim Zatni: Performed the experiments; Analysed and interpreted the data; Contributed reagents, materials, analysis tools or data.

Funding statement

This research did not receive any specific grant from funding agencies in the public, commercial, or not-for-profit sectors.

Data availability statement

No data was used for the research described in the article.

Declaration of competing interest

The authors declare that they have no known competing financial interests or personal relationships that could have appeared to influence the work reported in this paper.

References

[1] S. Sun, L. Zhu, Compact dual-band microstrip bandpass filter without external feeds, IEEE Microw. Wireless Compon. Lett. 15 (2005) 644–646, https://doi.org/10.1109/LMWC.2005.856687.
[2] L.K. Yeung, K. Wu, A dual-band coupled-line balun filter, IEEE Trans. Microw. Theor. Tech. 15 (2007) 2406–2411, https://doi.org/10.1109/TMTT.2007.907402.
[3] B. Wu, C. Liang, P. Qin, Q. Li, Compact dual-band filter using defected stepped impedance resonator, IEEE Microw. Wireless Compon. Lett. 18 (2008) 674–676, https://doi.org/10.1109/LMWC.2008.2003459.
[4] L. Gao, X.Y. Zhang, K.X. Wang, B. Hu, L. Gao, X.Y. Zhang, K.X. Wang, B. Hu, Miniaturized dual-band bandpass filter using quarter-wavelength stepped-impedance resonators, Asia *Pacific Microwave Conference Proceedings* (2012) 674–676, https://doi.org/10.1109/APMC.2012.6421558.

[5] H. Zhu, A.M. Abbosh, Single- and dual-band bandpass filters using coupled stepped-impedance resonators with embedded coupled-lines, IEEE Microw. Wireless Compon. Lett. 26 (2016) 675–677, https://doi.org/10.1109/LMWC.2016.2597180.
[6] I.-S. Kim, G. Kim, J.T. Park, Y.S. Jang, B.J. Park, Tri-section stepped impedance resonator with adjustable length and improved second harmonic characteristics, Microw. Opt. Technol. Lett. 62 (2020) 82–87, https://doi.org/10.1002/mop.31993.
[7] J.-S. Hong, S. Li, Theory and experiment of dual-mode microstrip triangular patch resonators and filters, IEEE Trans. Microw. Theory. 52 (2004) 1237–1243, https://doi.org/10.1109/TMTT.2004.825653.
[8] C.-H. Tseng, H.-Y. Shao, A new dual-band microstrip bandpass filter using net-type resonators, IEEE Microw. Wireless Compon. Lett. 20 (2010) 196–198, https://doi.org/10.1109/LMWC.2010.2042549.
[9] S. Sun, A dual-band bandpass filter using a single dual-mode ring resonator, IEEE Microw. Wireless Compon. Lett. 21 (2011) 298–300, https://doi.org/10.1109/LMWC.2011.2132119.
[10] J. Shi, L. Lin, J. Chen, H. Chu, X. Wu, Dual-band bandpass filter with wide stopband using one stepped-impedance ring resonator with shorted stubs, IEEE Microw. Wireless Compon. Lett. 24 (2014) 442–444, https://doi.org/10.1109/LMWC.2014.2316259.
[11] Dechen Ma, Zhong Yin Xiao, Liangliang Xiang, Xiaohuan Wu, Chunyan Huang, Xin Kou, Compact dual-band bandpass filter using folded sir with two stubs for WLAN, Progress In Electromagnetics Research 117 (2011) 357–364, https://doi.org/10.2528/PIER11040201.
[12] C.-H. Chen, C.-H. Huang, T.-S. Horng, S.-M. Wu, Highly miniaturized multiband bandpass filter design based on a stacked spiral resonator structure, IEEE Trans. Microw. Theor. Tech. 60 (2012) 1278–1286, https://doi.org/10.1109/TMTT.2012.2187797.
[13] X.Y. Zhang, J.-X. Chen, Q. Xue, S.-M. Li, Dual-band bandpass filters using stub-loaded resonators, IEEE Microw. Wireless Compon. Lett. 17 (2007) 583–585, https://doi.org/10.1109/LMWC.2007.901768.
[14] L. Gao, X.Y. Zhang, High-selectivity dual-band bandpass filter using a quad-mode resonator with source-load coupling, IEEE Microw. Wireless Compon. Lett. 23 (2013) 474–476, https://doi.org/10.1109/LMWC.2013.2274995.
[15] W. Jiang, W. Shen, T. Wang, Y.M. Huang, Y. Peng, G. Wang, Compact dual-band filter using open/short stub loaded stepped impedance resonators (OSLSIRs/SSLSIRs), IEEE Microw. Wireless Compon. Lett. 26 (2016) 672–674, https://doi.org/10.1109/LMWC.2016.2597179.
[16] M.-H. Weng, F.-Z. Zheng, H.-Z. Lai, S.-K. Liu, Compact ultra-wideband bandpass filters achieved by using a stub-loaded stepped impedance resonator, Electronics 9 (2020) 209, https://doi.org/10.3390/electronics9020209.
[17] Raaed T. Hammed, Saad M. Abbas, A small dual narrowband BPF with ultra-rejection band using grounded stepped impedance resonator, IETE J. Res. (2021), https://doi.org/10.1080/03772063.2021.1906337.
[18] J.-T. Kuo, E. Shih, Wideband bandpass filter design with three-line microstrip structures, Proc. Inst. Elect. Eng.–Microw. Antennas Propag 149 (2002) 243–247, https://doi.org/10.1049/ip-map:20020572.
[19] Z.G. Wang, R.M. Xu, B. Yan, A covering ka-band two-way switch filter module using a three-line and an E-plane waveguide band-pass filters, Int. J. RF Microw. Computer-Aided Eng. 25 (2015) 305–310, https://doi.org/10.1002/mmce.20863.
[20] D.M. Pozar, Microwave Engineering, second ed., John Wiley & Sons, Inc., Hoboken, NJ, USA, 1998.
[21] M. Makimoto, S. Yamashita, Bandpass filters using parallel coupled stripline stepped impedance resonators, IEEE Trans. Microw. Theor. Tech. 12 (1980) 1413–1417, https://doi.org/10.1109/TMTT.1980.1130258.
[22] V.K. Tripathi, On the analysis of symmetrical three-line microstrip circuits, IEEE Trans. Microw. Theor. Tech. 25 (1977) 726–729, https://doi.org/10.1109/TMTT.1977.1129202.
[23] D. Pavlidis, H.L. Hartnagel, The design and performance of three-line microstrip couplers, IEEE Trans. Microw. Theor. Tech. 24 (1976) 631–640, https://doi.org/10.1109/TMTT.1976.1128928.
[24] Dal Ahn, , Chul-Soo Kim, Min-Ho Chung, Dwong-Hwan Lee, Dae Won Lew, Heon Jin Hong, The design of parallel coupled line filter with arbitrary image impedance, IEEE MTT-S International Microwave Symposium Digest 2 (1998) 909–912, https://doi.org/10.1109/MWSYM.1998.705138.
[25] Jen-Tsai Kuo, M. Jiang, Hsien-Jen Chang, Design of parallel-coupled microstrip filters with suppression of spurious resonances using substrate suspension, IEEE Trans. Microw. Theor. Tech. 52 (2004) 83–89, https://doi.org/10.1109/TMTT.2003.821247.
[26] H. Zhang, W. Kang, W. Wu, Dual-band substrate integrated waveguide bandpass filter utilising complementary split-ring resonators, Electron. Lett. 54 (2018) 85–87, https://doi.org/10.1049/el.2017.3478.
[27] Y. Xie, F. Chen, Z. Li, Design of dual-band bandpass filter with high isolation and wide stopband, IEEE Access 5 (2017) 25602–25608, https://doi.org/10.1109/ACCESS.2017.2773502.
[28] F. Wei, J.H. Yu, C.Y. Zhang, C. Zeng, X.W. Shi, Compact balanced dual-band BPFs based on short and open stub loaded resonators with wide common-mode suppression, IEEE Transactions on Circuits and Systems II: Express Briefs 67 (2020) 3043–3047, https://doi.org/10.1109/TCSII.2020.2994632.
[29] Jessada Konpang, Natchayathorn Wattikornsirikul, Dual-mode dual-band bandpass filter with high cutoff rejection by using asymmetrical transmission zeros technique, Progress In Electromagnetics Research M 100 (2021) 225–236, https://doi.org/10.2528/PIERM20102302.
[30] Y.X. Wang, Y.Li Chen, W.H. Zhou, W.C. Yang, J. Zen, Dual-band bandpass filter design using stub-loaded hairpin resonator and meandering uniform impedance resonator, Progress In Electromagnetics Research Letters 95 (2021) 147–153, https://doi.org/10.2528/PIERL20102102.